Stellar counter-rotation in lenticular galaxy NGC 448

Ivan Yu. Katkov,[1]⋆ Olga K. Sil'chenko,[1,2]⋆ Igor V. Chilingarian,[1,3]⋆
Roman I. Uklein[4] and Oleg V. Egorov[1]

[1]*Sternberg Astronomical Institute, M.V. Lomonosov Moscow State University, Universitetskiy pr., 13, Moscow 119992, Russia*
[2]*Isaac Newton Institute of Chile, Moscow Branch*
[3]*Smithsonian Astrophysical Observatory, Harvard-Smithsonian Center for Astrophysics, 60 Garden St MS09, Cambridge, MA 02138, USA*
[4]*Special Astrophysical Observatory, Nizhniy Arkhyz, Karachai-Cherkessia 369167, Russia*

ABSTRACT

The counter-rotation phenomenon in disc galaxies directly indicates a complex galaxy assembly history which is crucial for our understanding of galaxy physics. Here, we present the complex data analysis for a lenticular galaxy NGC 448, which has been recently suspected to host a counter-rotating stellar component. We collected deep long-slit spectroscopic observations using the Russian 6-m telescope and performed the photometric decomposition of Sloan Digital Sky Survey archival images. We exploited (i) a non-parametric approach in order to recover stellar line-of-sight velocity distributions and (ii) a parametric spectral decomposition technique in order to disentangle stellar population properties of both main and counter-rotating stellar discs. Our spectral decomposition stays in perfect agreement with the photometric analysis. The counter-rotating component contributes ≈30 per cent to the total galaxy light. We estimated its stellar mass to be $9.0^{+2.7}_{-1.8} \times 10^9 \, M_\odot$. The radial scalelength of counter-rotating disc is ≈3 times smaller than that of the main disc. Both discs harbour old stars but the counter-rotating components reveal a detectable negative age gradient that might suggest an extended inside-out formation during 3...4 Gyr. The counter-rotating disc hosts more metal-rich stars and possesses a shallower metallicity gradient with respect to the main disc. Our findings rule out cosmological filaments as a source of external accretion which is considered as a potential mechanism of the counter-rotating component formation in NGC 448, and favour the satellite merger event with the consequent slow gas accretion.

Key words: galaxies: elliptical and lenticular, cD – galaxies: evolution – galaxies: individual: NGC 448 – galaxies: ISM – galaxies: kinematics and dynamics.

1 INTRODUCTION

The kinematical appearance, as well as the stellar population properties keep a fossil record about the process of galaxy assembly which is crucial for our understanding of galaxy physics. Most disc galaxies possess regular rotation but systems with peculiar kinematics are also observed. Rubin (1994) proposed a term 'multispin galaxies' for objects possessing embedded kinematically decoupled components, the angular momentum of which differs from that of the host galaxy. The class of multispin galaxies includes objects with various kinematically distinct components containing gas and/or stars having different spatial extent and inclination with respect to the main galaxy disc: inner polar discs, extended polar rings/discs, moderately inclined rings, kinematically decoupled cores, and extended counter-rotating components.

Studies of multispin components shed the light on the process of gas accretion and merging history which are thought to be responsible for shaping disc galaxies. The stellar counter-rotation confined to the main galactic plane can be considered as a final product of evolution of externally acquired gas that has been processed through at least two major steps: (i) settling of the gas into the equatorial galactic plane due to, for instance, dynamical influence of the gravitational potential of the main disc (Tohline, Simonson & Caldwell 1982); (ii) and subsequent star formation (Pizzella et al. 2004). Potentially, studies of counter-rotating components may allow us to date accretion events and the following star formation that leads to understanding of the galaxy assembly.

The counter-rotation phenomena were deeply studied by means of numerical simulations, Thakar & Ryden (1996, 1998) investigated various mechanisms which are able to produce a counter-rotating gas component, such as episodic and continuous gas infall or merger with a gas-rich dwarf satellite. In their simulations, only small counter-rotating stellar discs with radial density profiles different from exponential were generated. Binary major mergers

⋆E-mail: katkov@sai.msu.ru (IYK); sil@sai.msu.ru (OKS); igor.chilingarian@cfa.harvard.edu (IVC)

of giant galaxies usually destroy discs and form ellipticals (Barnes & Hernquist 1991). However, a strictly coplanar merger of two gas-rich giant progenitor galaxies is able to build up a massive counter-rotating disc (Puerari & Pfenniger 2001; Crocker et al. 2009). Otherwise, recent numerical cosmological simulation by Algorry et al. (2014) naturally predicts the formation of counter-rotating discs as a consequence of gas accretion from two distinct filamentary structures.

Presently, several dozens of galaxies with counter-rotating components are known (Galletta 1996; Corsini 2014). The majority of them have been only suspected to host counter-rotating components. Particular progress in the studies of counter-rotating discs has been achieved upon development of the spectral decomposition approaches. For the first time, such an approach was applied by Chilingarian et al. (2011) in order to recover a spectrum of an ultracompact dwarf galaxy contaminated by the host galaxy light. Independently, Coccato et al. (2011) first proposed the spectral decomposition approach based on the spectral pixel fitting technique PPXF (Cappellari & Emsellem 2004) for the investigation of the counter-rotation in NGC 5719. The spectral decomposition allows one to disentangle contributions of both counter-rotating and main components to the observed spectrum and to determine stellar population properties and, therefore, constrain their formation mechanisms. Coccato et al. (2011) simultaneously measured kinematics and stellar population properties and found that less-massive counter-rotating component is younger, less metal abundant and α-element enhanced with respect to the main stellar disc. Later, Coccato et al. and other teams, including ours, analysed spectra of a few counter-rotating galaxies by using the same or similar approaches. The disc galaxies with counter-rotation, NGC 3593, NGC 4138, NGC 4191, NGC 4550, NGC 5719, and IC 719, have been studied in this manner (Coccato et al. 2011, 2013, 2015; Johnston et al. 2013; Katkov, Sil'chenko & Afanasiev 2013; Pizzella et al. 2014). The results of these studies indicate that the counter-rotating components in all those objects being less massive than the main stellar discs, have younger stellar populations than the main discs while their metallicities and α-element abundances can deviate in both directions. Those findings are in agreement with the formation scenario where counter-rotating stars emerge from the externally accreted gas (Pizzella et al. 2004).

In this paper, we expand the sample of well-studied counter-rotating galaxies by one more object. We present an analysis of new deep long-slit spectroscopic data for a counter-rotating lenticular galaxy NGC 448.

2 NGC 448: GENERAL DESCRIPTION

NGC 448 is a lenticular galaxy located at a distance of 29.5 Mpc (Cappellari et al. 2011) with the total luminosity $M_B = -19.17$ mag (according to the HyperLeda data base,[1] Paturel et al. 2003) and $M_K = -23.02$ mag, Cappellari et al. 2011. In the RC3 (de Vaucouleurs et al. 1991), NGC 448 is classified as S0^- edge-on. Nevertheless, the direct Sloan Digital Sky Survey (SDSS) image (Fig. 1) does not explicitly indicate a strongly edge-on galaxy orientation.

NGC 448 was included into the ATLAS[3D] integral-field spectroscopic survey (Cappellari et al. 2011). For the first time, NGC 448 was noticed as a galaxy possessing two large-scale counter-rotating disc-like stellar components by Krajnović et al. (2011) basing on ATLAS[3D] stellar line-of-sight velocity and velocity dispersion maps
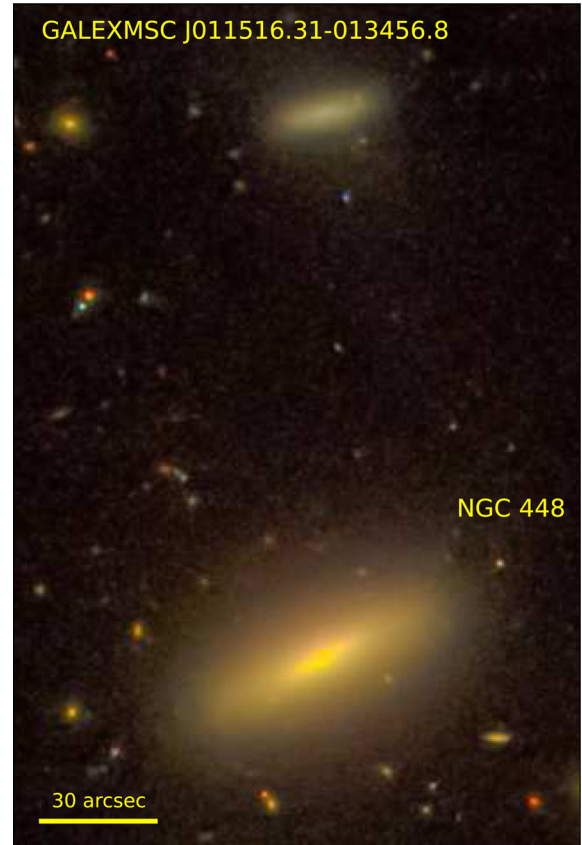
Figure 1. Coloured SDSS (DR12; Alam et al. 2015) image of NGC 448 and its satellite GALEXMSC J011516.31−013456.8. North is up, east is left. The image was extracted using the cutout image service (SDSS image cutout tool http://skyserver.sdss.org/dr12/en/help/docs/api.aspx#cutout).

which indicate a counter-rotating core and double-peak features, correspondingly.

NGC 448 has a companion galaxy 2.6 arcmin to the north which corresponds to the projected separation of 22 kpc for the adopted galaxy distance of 29.5 Mpc. According to the NASA/IPAC Extragalactic Database (NED),[2] this galaxy is cross-identified with GALEXMSC J011516.31−013456.8, which radial velocity $v_r = 22105\,\mathrm{km\,s^{-1}}$ was determined in the Cluster and Infall Region Nearby Survey project (Rines et al. 2003). However, extremely deep optical imaging with the MegaCam camera at the Canada–France–Hawaii Telescope unambiguously shows a tidal interaction between NGC 448 and a disturbed companion (see fig. 16 in Duc et al. 2015[3]). One can see a faint tidal tail around GALEXMSC J011516.31−013456.8 even at the contrast-enhanced SDSS image (Fig. 1). This points to the wrong redshift measurement for GALEXMSC J011516.31−013456.8 and suggests the physical interaction between this galaxy and NGC 448.

Investigation of stellar population properties by using optical long-slit spectra revealed the old stellar population (∼9 Gyr) and slightly subsolar metallicity in NGC 448 (Caldwell, Rose & Concannon 2003). Similar values were determined by McDermid et al. (2015) based on the SAURON Lick index measurements

---

within one effective radius ($R_{\rm eff} = 11.2$ arcsec): $T_{\rm SSP} = 8.0 \pm 1.5$ Gyr, $Z_{\rm SSP} = -0.21 \pm 0.05$ dex, $[\alpha/{\rm Fe}] = 0.1 \pm 0.06$ dex. Observations of the CO emission provides only upper limits on the mass of molecular hydrogen, $M({\rm H}_2) < 5.5 \times 10^7$ M$_\odot$, (Young et al. 2011). We do not find any data on the H I content of NGC 448.

3 DATA ANALYSIS

3.1 Observations and data reduction

We obtained new deep spectroscopic data for NGC 448 on 2013 October 25 by using the Spectral Camera with Optical Reducer for Photometric and Interferometric Observations (SCORPIO) universal spectrograph (Afanasiev & Moiseev 2005) mounted at the prime focus of the Russian 6-m BTA telescope operated by the Special Astrophysical Observatory. We used the long-slit mode with the slit width of 1.0 arcsec placed along the major axis of the galaxy. The volume phase holographic grism VPHG2300G gives the spectral resolving power $R \approx 2000$ (instrumental velocity dispersion of $\sigma_{\rm inst} \approx 65$ km s^{-1}) in the wavelength range 4800. . . 5600 Å which includes strong absorption (Mgb, Fe5270, Fe5335, etc.) and emission lines (Hβ, [O III], [N I]). We collected 16 exposures of 15 min each (4 h in total) under good atmospheric transparency with the average seeing of 1.5 arcsec full width at half-maximum (FWHM). The detector CCD EEV42-40 (2048 × 2048 pixels) provides the spectral sampling of 0.37 Å pix^{-1} and the slit plate scale of 0.357 arcsec pix^{-1} in the 1 × 2 binning mode. In addition to the science spectra, we obtained internal flat-field, arcs (He–Ne–Ar) and twilight spectra.

We reduced our spectroscopic data with our own IDL-based pipeline which consists of standard procedures such as bias subtraction, flat-fielding, cosmic ray hit rejection by using Laplacian filtering technique L.A.Cosmic (van Dokkum 2001), the wavelength calibration, the sky background subtraction and correction for the spectral sensitivity inhomogeneity. In order to build the wavelength solution, we fitted the arc line positions using bivariate polynomial of the fifth degree along dispersion and the fourth degree across dispersion in order to take into account the slit image curvature. A typical value of the rms in every line is 0.05 Å. Due to optical distortions, the spectral line spread function (LSF) of the spectrograph varies along the slit as well as within the wavelength range. The LSF variations affect the night-sky spectrum which is derived by using outer areas of the frame, where LSF shape differs from that in the regions of the galaxy close to the slit centre. In order to take into account LSF variations, we used the reconstruction method in the Fourier space described in Katkov, Sil'chenko & Afanasiev (2014); a detailed discussion on the sky subtraction for a changing LSF is provided in Chilingarian et al. (2009) and Katkov & Chilingarian (2011). Finally, we linearized the spectra and integrated all separate exposures controlling the position of the bright galaxy centre in order to take into account the atmospheric refraction. We computed error frames from the photon statistics and proceeded them through all reduction steps. We exploited the twilight spectrum in order to extract the LSF along the slit by fitting it against a high-resolution solar spectrum.

Fig. 2 demonstrates a fragment of the co-added reduced spectrum of NGC 448 near the strong Mgb absorption feature. The spectrum is normalized by mean values in every row along the slit for presentation purposes in order to achieve the higher contrast. The complex velocity structure of the absorption lines which corresponds to kinematically separated stellar components is clearly seen.
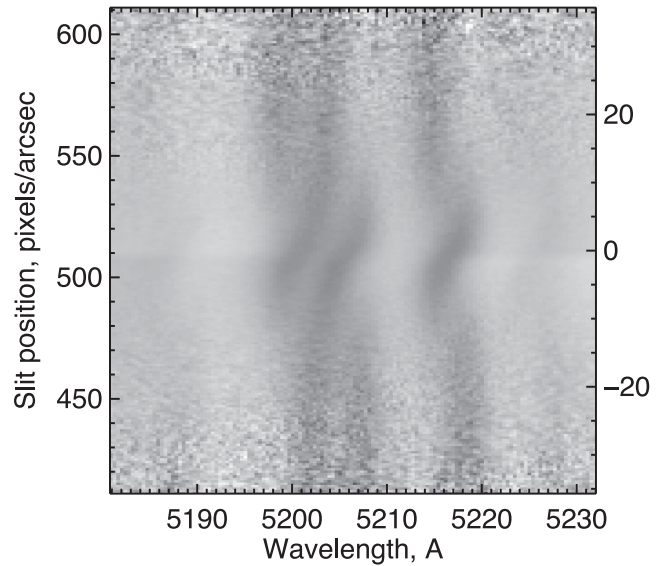
Figure 2. Fragment of the long-slit spectrum around the Mgb absorption feature. In order to achieve a better contrast, the spectrum was normalized by the average light profile. Two kinematically distinguished components are clearly seen.

3.2 The non-parametric LOSVD reconstruction

A visual inspection of strong absorption lines in the spectrum (see Fig. 2) reveals a complex, multicomponent structure of the line-of-sight velocity distribution (LOSVD) of stars which cannot be successfully described by a single Gaussian or a Gaussian–Hermite function (van der Marel & Franx 1993).

We applied a non-parametric reconstruction approach in order to determine the stellar LOSVD of NGC 448. First, we adaptively bin the long-slit spectrum in the spatial direction in order to reach a minimal signal-to-noise ratio of S/N = 30 per bin per spectral pixel in the middle of the spectral range. After that, we determine a template spectrum by using the NBURSTS package (Chilingarian et al. 2007a,b). This package implements a pixel-to-pixel χ^2 minimization fitting algorithm, where an observed spectrum is approximated by a stellar population model broadened with a parametric LOSVD (the Gaussi–Hermite shape is used at this step) and multiplied by some polynomial continuum in order to take into account dust attenuation and/or possible flux calibration errors in both observations and models. We used a grid of PEGASE.HR high-resolution simple stellar population (SSP) models (Le Borgne et al. 2004) based on the ELODIE3.1 empirical stellar library (Prugniel et al. 2007), the Salpeter initial mass function (IMF) and pre-convolved with the SCORPIO LSF determined from a twilight spectrum as explained above. Then, we used the stellar population model broadened with the LSF only (without the LOSVD) as a template spectrum for the non-parametric LOSVD reconstruction. The reconstruction technique does not require any a priori knowledge about the LOSVD shape and searches the solution of the convolution problem as a linear inverse ill-conditioned problem by using a smoothing regularization. For more details, see Katkov et al. (2013) and Katkov et al. (2011) where we applied the same approach to recover a counter-rotating stellar disc in the lenticular galaxy IC 719 and a complex LOSVD in NGC 524.

Fig. 3 shows the reconstructed non-parametric stellar LOSVD of NGC 448 for each spatial bin. Again a complex two-component peaked structure is clearly visible. Then, we fitted a non-parametric
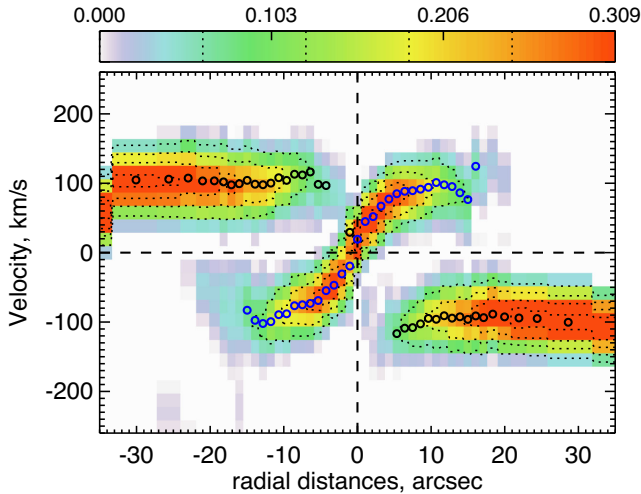
Figure 3. Our result of the non-parametric reconstruction of the stellar LOSVD presented as a position–velocity diagram. Black and blue circles show Gaussian peak positions for a double Gaussian decomposition.

LOSVD by a combination of two Gaussians in every bin and estimated the line-of-sight velocities and stellar velocity dispersions for the two kinematically distinct components.

3.3 The parametric spectral decomposition

In order to study stellar population properties of the counter-rotating and main stellar components, we separated their contributions to the integrated spectrum by using the two-component mode of the NBURSTS package. In general, we fitted an observed spectrum by a linear combination of two SSP templates, each characterized by its own age and metallicity, and broadened by different Gaussian-shaped LOSVDs. The multiplicative polynomial continuum was the same for both components. The Gaussian parameters of the previous non-parametric LOSVD decomposition were used as an initial guess for the kinematics of components. Finally, the free parameters of our model are line-of-sight (LOS) velocity, velocity dispersion, age, metallicity for every component, relative weights and the 15th order the polynomial continuum, hence, 24 parameters in total. Thanks to the high-signal-to-noise ratio and relatively high spectral resolution, the fitting procedure was stable enough so we did not have to fix any parameters of the model. In order to estimate the parameter uncertainties, we ran a Monte Carlo simulation for a hundred realization of synthetic spectra for each spatial bin which were created by adding a random noise corresponding to the signal-to-noise ratio in the bin to the best-fitting model.

Fig. 4 shows an example of a spectrum with the overplotted best-fitting model in a region where the complex two-component structure of absorption lines is clearly seen. The decomposed radial profiles of the kinematics and stellar populations are shown in the Fig. 5.

3.4 The photometric decomposition

As a complementary approach to the spectroscopic decomposition, we performed a two-dimensional (2D) decomposition of an SDSS *g*-band image of NGC 448. We used the *g* band in order to compare the photometric decomposition results with those obtained from the spectra since the spectral range of our observations is close to the SDSS *g* band.
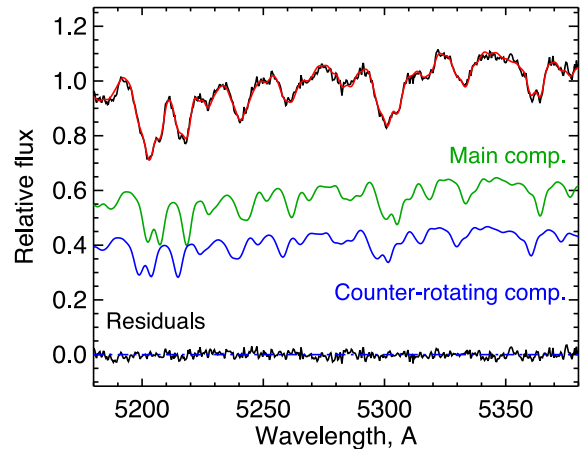
Figure 4. Fragment of the spectrum at a radius $r = -12$ arcsec. The red line corresponds to the best-fitting model overplotted on top of the observed spectrum. Green and blue lines show the main disc and the counter-rotating component, correspondingly.

In order to construct a photometric model of the galaxy, we used the GALFIT (Peng et al. 2010) software. An accurate treatment of uncertainties, both for the galaxy image and for the point spread function (PSF), is required in order to obtain reliable component parameters of the photometric model when using GALFIT. We took into account the image uncertainties following the SDSS documentation.[4] The PSF function was determined by the SEXTRACTOR/PSFEx packages (Bertin & Arnouts 1996; Bertin 2011). We masked background/foreground interlopers (stars, galaxies) superimposed on the galaxy by using the fitting residuals map and then repeated the fitting process.

The field around NGC 448 is crowded because of Galactic foreground stars. That could potentially lead to the imperfect sky subtraction and, consequently, bias the photometric decomposition. We re-analysed the sky unsubtracted SDSS image (constructed according to the published documentation[4]) and estimated the sky level by using azimuthally averaged surface brightness profile determined by fitting ellipses with constant ellipticity and position angle at large radii from the galaxy centre (150–200 arcsec). We found that our sky background estimate differs from the SDSS pipeline value[5] by 0.2 per cent which stays within uncertainties of our background estimate.

We performed numerous tests and found that the galaxy image can be successfully decomposed into four components: a Sérsic nuclear core, two exponential discs and a halo described also by a Sérsic function.

Beside this model, we tested other photometric decompositions: (i) 2 Sérsic + exponential disc + edge-on disc; and (ii) 2 Sérsic + exponential disc. In order to choose between models and to measure quantitatively how well those models fit the same data, we compared normalized χ^2 values, the Akaike and Bayesian information criteria (AIC, Akaike 1974; BIC, Schwarz 1978) which we present in the Table 1. The model with the lowest AIC or BIC is preferred, though a difference ΔAIC or ΔBIC of at least ∼6 is usually required before one model can be deemed clearly superior (Erwin 2015).

---

[4] http://data.sdss3.org/datamodel/files/BOSS_PHOTOOBJ/frames/RERUN/RUN/CAMCOL/frame.html

[5] The SDSS pipeline produces bivariate sky map. To compare it with our sky-level estimate, we averaged this map within the galaxy area, which is used for the photometric decomposition.
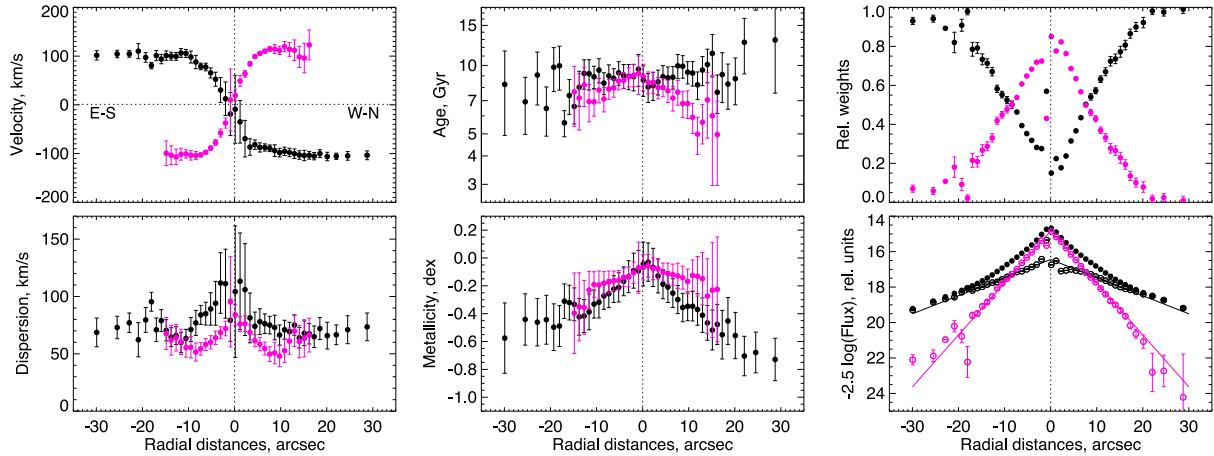
Figure 5. The spectral decomposition results for NGC 448. Black symbols correspond to the main stellar component, magenta symbols to the counter-rotating disc. Left-hand panels show radial profiles of the line-of-sights velocity (top) and the stellar velocity dispersion (bottom). Middle panels: SSP equivalent stellar population ages (top) and metallicities (bottom). Right-hand panels: relative contribution of every component to the integrated spectrum (top); the bottom panel shows the light profile which was obtained by integrating the spectra along the slit (filled symbols) and light profiles of each component (open symbols).

Table 1. Statistical tests of photometric models.

Model	χ^2/DOF	$\Delta\mathrm{BIC}$	$\Delta\mathrm{AIC}$
2 Sérsic + 2 Exp. disc	1.058	0.0	0.0
2 Sérsic + Exp. disc + Edge-on disc	1.068	656.1	665.2
2 Sérsic + Exp. disc	1.146	5984.7	6048.8

Finally, we adopted a four-component model that consists of a Sérsic nuclear core, two exponential discs, and a Sérsic halo. Hereafter, the more centrally concentrated exponential disc is referred to as 'CR' assuming its association with the counter-rotating stellar component. Fig. 6 graphically demonstrates the results of the decomposition, and Fig. 7 displays the comparison between the spectroscopic and photometric results. Table 2 presents the best-

fitting parameters of the photometric model as well as parameter uncertainties. We estimated the parameter uncertainties from the co-variance matrix as a standard output of the Levenberg–Marquardt minimization algorithm used in the GALFIT routine and also by Monte Carlo simulations for a hundred realizations of synthetic galaxy images in the same manner as for the spectroscopic decomposition. Error estimates from both approaches are in good agreement. We emphasize that our uncertainty estimates should probably be considered as lower limits of the true parameter uncertainties (Häussler et al. 2007; Erwin 2015) and should be used with caution.

3.5 Results

It is clearly seen on the position–velocity diagram (Fig. 3) as well as on the radial profiles of the light contribution of the individual
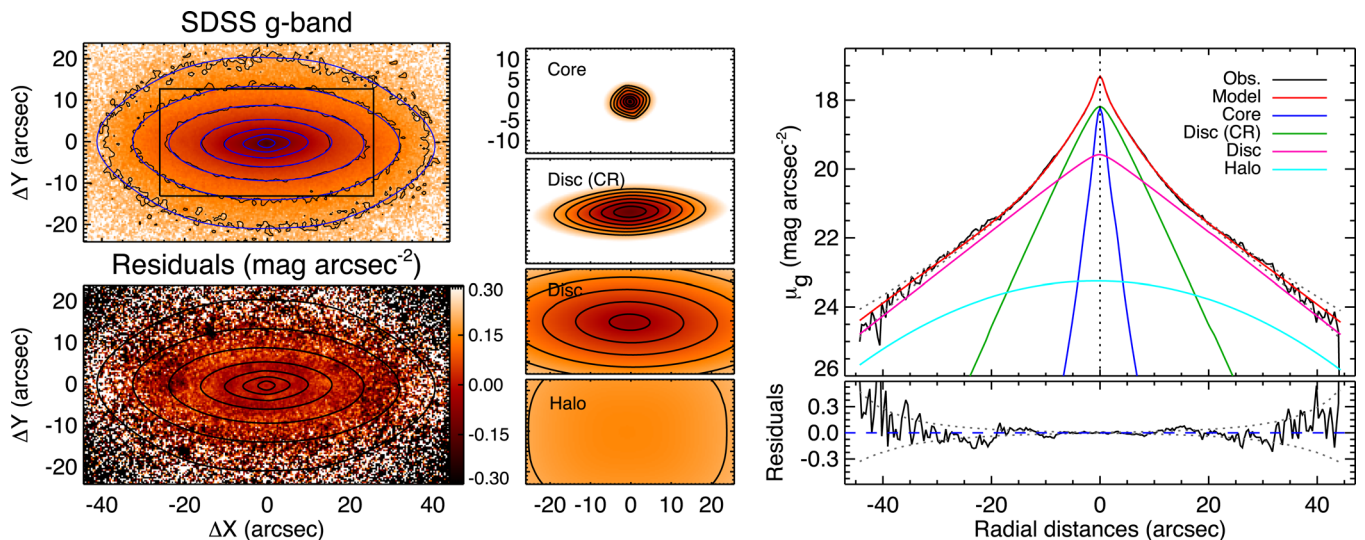
Figure 6. The 2D photometric decomposition results of the SDSS *g*-band image. The top panel in the left block presents the galaxy image superimposed by contours according to the surface brightness of 18, 19, 20, 21, 22, 23, 24 mag arcsec^{-2}. Blue lines correspond to the contours of the model image. The bottom panel in the left block presents a residual map in magnitudes with the model contours as a reference. The middle block shows images of the model subcomponents (from top to bottom): core, disc (CR), main disc, halo. The right block presents a 1D light profile along the major axis of the galaxy (black line) with the overplotted total four-component model (in red) and the subcomponent profiles (in colours). Dotted lines show the level of uncertainties. The bottom panel in this block corresponds to the fitting residuals.
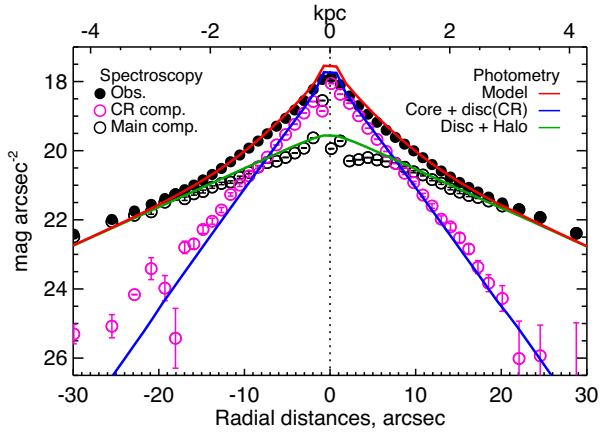
Figure 7. Comparison of the photometric and spectroscopic decompositions. Filled circles show the light profile extracted from our long-slit spectrum, open circles are the results of the spectroscopic decomposition on the main (in black) and counter-rotating (in magenta) components. Solid lines display the result of the photometric decomposition. The red solid line corresponds to the total photometric model, the blue solid line is a sum of disc (CR) and core components that is assumed to be associated with the counter-rotating component, the green solid line is a main component represented by the sum of the main disc and halo components. Here, we took into account the atmospheric seeing difference between SCORPIO observations (FWHM = 1.5 arcsec) and SDSS *g*-band image (FWHM = 1.0 arcsec) as well as sampling effects. This comparison clearly demonstrates the successful agreement between spectroscopic and photometric approach.

components extracted from the long-slit data (the right-hand panel of Fig. 5) that the counter-rotating component dominates in the integrated spectrum in the central region of NGC 448. The total light fraction of the counter-rotating disc within one effective radius ($R_{\rm eff} = 11.2$ arcsec) is 60 per cent and decreases to 45 per cent within $2R_{\rm eff}$ (see Fig. 8).

Our photometric results completely agree with the spectral decomposition. Fig. 7 demonstrates the comparison of the major axis light profiles extracted from the spectrum and from the image. Note, that in the central region we cannot separate the contributions of the kinematical components due to the very small difference of their line-of-sight velocities. Therefore, it is more reasonable to compare the total contribution of the CR disc *and* the core component together. Fig. 8 shows the comparison of the total light fraction of the counter-rotating component within a given galactocentric radius.

We assume that the counter-rotating component has a disc morphology. This assumption is supported by a relatively low velocity dispersion ($V/\sigma \sim 2$) and by the exponential shape of the light profile distribution (see the right-hand panel of Fig. 5). Our 2D photometric model of NGC 448 contains two exponential discs. In our photometric model, the counter-rotating disc (CR) has a significant diskiness of isophotes which is characterized by $C_0 = 0.2$. The nearly edge-on disc orientation can produce such values of the C_0 coefficient. The GALFIT package contains the edge-on disc model. We tested it and found that it yields higher values of χ^2 as well as the statistical criteria AIC and BIC which may be connected to the disc thickness changing along the radius.

We cannot determine the exact orientation of the counter-rotating disc with respect to the main disc by relying only on our long-slit kinematical data because we observed NGC 448 only in one slit position. However, there are several arguments which support the discs to be settled in the same plane: (i) the equal amplitudes of the line-of-sight velocity variations along the radius; (ii) the co-alignment of the kinematical major axes of the central counter-rotating region and the outermost main disc component (see ATLAS[3D] velocity maps in Krajnović et al. 2011); (iii) similar values of the isophote major axis position angles and inclinations.[6]

We found that in the galaxy centre both discs contain old stars ($T_{\rm SSP} \approx 9$ Gyr) having subsolar metallicity putting our results in agreement with the literature (Caldwell et al. 2003; McDermid et al. 2015). Our deep spectroscopic data allowed us to determine a noticeable age gradient $\Delta\log T_{\rm CR} = -0.087 \pm 0.026$ dex dex^{-17} in the counter-rotating stellar disc, while in the main stellar disc the age profile is flat ($\Delta\log T_{MD} = -0.009 \pm 0.024$ dex dex^{-1}). The stellar metallicity gradients are also noticeably different: $\Delta\log Z_{\rm CR} = -0.09 \pm 0.04$ dex dex^{-1} while $\Delta\log Z_{MD} = -0.33 \pm 0.05$ dex dex^{-1}.

We have subtracted the best-fitting absorption-line model from the observed spectrum in order to obtain a pure emission-line spectrum. Our long-slit spectrum covers the positions of the H β and [O III] emission lines. We have not detected any significant signal in these lines.

Although we have not clearly detected emission lines in the spectra of NGC 448, we found signs of possible star formation in infrared (IR) images. We analysed available archival *Spitzer* images of the galaxy at 3.6μ and 8μ. While emission in the first band originates almost exclusively from the stellar light, the dominate sources of emission at 8μ are polycyclic aromatic hydrocarbons, being excited by UV photons from massive and/or hot stars. Hence, if bright emission is seen in an 8μ image after the subtraction of the stellar population contribution, this should indicate the presence of gas excited either by the star formation in a galaxy or by hot-evolved blue horizontal branch stars. In order to subtract the stellar continuum in the 8μ image, we used the calibration by Ciesla et al. (2014) that estimated the 8μ stellar contribution to be about 24.9 per cent of the total flux at 3.6μ for early-type galaxies. The subtracted image corresponding to the non-stellar emission at 8μ is shown in Fig. 9 with overlaid contours from the optical SDSS-*g* image.

We calculated the stellar mass of the counter-rotating component by using mass-to-light ratios (M/L) determined from spectral fitting based on the PEGASE.HR models with the Salpeter IMF and the light profile which we recovered from the photometry. As we described above the counter-rotating component is assumed to be associated with both the core and the CR disc components in the photometric decomposition. Since the core is very centrally concentrated, we used a single stellar mass-to-light ratio of $(M/L_g)_{\rm core} = 6.3$ that corresponds to the central stellar population properties. For the disc (CR) component, we estimated $(M/L_g)_{\rm disc}$ pixel-by-pixel by using the gradients of the stellar population parameters retrieved from the long-slit spectrum. The total mass of the counter-rotating component is expected to be $M_{\rm CR} = 9.0^{+2.7}_{-1.8} \times 10^9\,{\rm M}_\odot$ including $M_{\rm disc} = 7.1^{+2.6}_{-1.8} \times 10^9\,{\rm M}_\odot$ and $M_{\rm core} = 1.8^{+0.2}_{-0.2} \times 10^9\,{\rm M}_\odot$. Mass uncertainties have been calculated by using uncertainties of the stellar population properties.

---

[6] Indeed, assuming flatnesses of the discs the axis ratios $q_{\rm CR} = 0.280$ and $q = 0.367$ produce inclinations $i_{\rm CR} = \arccos(q_{\rm CR}) = 74°$ and $i = 68°$, respectively

[7] The gradient calculated as a slope of a linear fit of the form $a + b\log(r/R_{\rm eff})$. The uncertainties of age and metallicity measurements are invoked to the χ^2 minimization routine to estimate 1σ error of the gradient.

Table 2. Structural component parameters of NGC 448 from the photometric decomposition. Column (2) corresponds to the central surface brightness μ_0, (3) is the disc scalelength h or effective radius r_e for Sérsic component, (4) is the Sérsic index n, (5) is the positional angle PA, (6) is the axis ratio $q = b/a$, (5) is the diskiness/boxiness C_0, (6) is the contribution to the total image (C/T). The parameter uncertainties outcome from GALFIT routine, while errors in the parentheses are extracted by means of Monte Carlo simulations.

Name	μ_0 (mag arcsec^{-2})	h, r_e (arcsec)	n	q	PA (deg)	C_0	C/T
(1)	(2)	(3)	(4)	(5)	(6)	(7)	(8)
Core	$17.25 \pm 0.21(0.25)$	$0.86 \pm 0.05(0.11)$	$1.86 \pm 0.14(0.19)$	$0.724 \pm 0.010(0.013)$	$122.37 \pm 1.43(1.13)$	–	0.05
Disc$_{CR}$	$19.75 \pm 0.01(0.02)$	$3.13 \pm 0.01(0.02)$	–	$0.279 \pm 0.002(0.04)$	$118.33 \pm 0.03(0.05)$	$0.19 \pm 0.02(0.03)$	0.27
Disc	$21.68 \pm 0.01(0.01)$	$8.84 \pm 0.05(0.05)$	–	$0.368 \pm 0.001(0.002)$	$115.09 \pm 0.04(0.04)$	$0.05 \pm 0.01(0.01)$	0.51
Halo	$25.56 \pm 0.06(0.07)$	$24.21 \pm 0.27(0.20)$	$0.49 \pm 0.01(0.02)$	$0.766 \pm 0.008(0.010)$	$116.02 \pm 0.70(0.59)$	$0.71 \pm 0.07(0.10)$	0.17
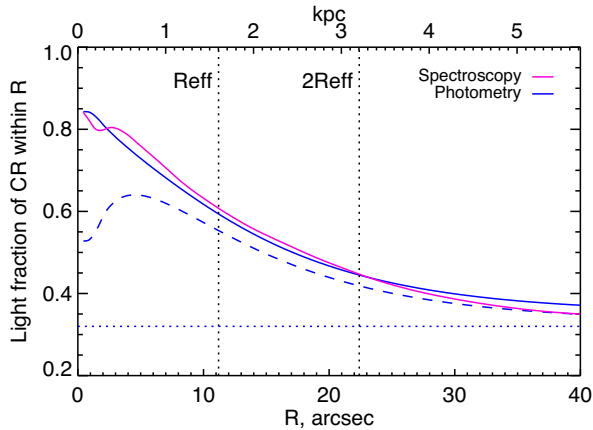
Figure 8. Total light fraction of the counter-rotating component (CR) within the galactocentric (not projected) radius R, which is calculated based on the light profiles extracted along the major axis from the long-slit spectroscopic decomposition (magenta) and from the 2D photometric decomposition (blue). The dashed blue line corresponds to the fraction of the Disc$_{CR}$ component only, while the solid blue line shows Disc$_{CR}$ + Core. The blue dotted horizontal line presents a total contribution of the CR component (Disc$_{CR}$ + Core) to the galaxy image from the GALFIT modelling. Note that we calculated the light fraction from 1D light profiles assuming an axisymmetric galaxy light distribution.

Figure 9. A stellar continuum subtracted *Spitzer* image at 8μ with overlaid contours according to the surface brightness values of 18, 19, 20, 21, 22, 23, 24 mag arcsec^{-2}. Some non-stellar signal is seen in the central part, $R < 10$ arcsec.

4 DISCUSSION AND CONCLUSIONS

The main challenge in the studies of galaxies possessing counter-rotating components is to establish a possible source of material with a different direction of the angular momentum and to clarify at least some details of the counter-rotating disc formation.

It is generally accepted that the presence of counter-rotating stars within the main stellar disc is a result of external material acquisition (Corsini 2014). Nevertheless, Evans & Collett (1994) suggested a scenario of internal origin of counter-rotating stars where stars take retrograde orbits during the bar dissolution process (separatrix crossing). From the stellar population point of view, only counter-rotating stellar discs with identical stellar population properties can be produced in the framework of this scenario. Hence, we decline it in the case of NGC 448 because the two discs have significantly different stellar population properties. Moreover, Evans & Collett (1994) suggested the separatrix crossing as a natural mechanism for building identical (with the same ages and scale lengths) counter-rotating discs in NGC 4550. However, the applicability of such mechanism for counter-rotating discs with very different scalelengths is not obvious.

Many recent detailed studies of disc galaxies with large-scale counter-rotating components support the external origin of counter-rotating stars. In all studied galaxies, stellar population properties derived from the spectra play an important role. It has been shown that the counter-rotating components detected in NGC 3593, NGC 5719, NGC 4191, NGC 4550, and IC 719 (Coccato et al. 2011, 2013, 2015; Johnston et al. 2013; Katkov et al. 2013) have younger stellar populations compared to the main stellar discs, and their ionized gas rotates in the same direction as the secondary stellar components, i.e. it also counter-rotates with respect to the main disc. These findings favour the scenario where counter-rotating stars have been formed *in situ* from the externally accreted gas.

Cosmological filaments and gas-rich satellites are considered as main candidate sources of external cold gas. However, it is often difficult to unambiguously disentangle between them. In both scenarios, one can expect to find either metal-poor or metal-rich counter-rotating stellar population with respect to the main disc, depending on the star formation history while the brief duration of the subsequent star formation event results in the α-element enhancement. The diversity of properties is observed. For instance, NGC 3593 and NGC 5719 indicate lower stellar metallicity in their counter-rotating discs with respect to the main discs while for NGC 4550 and NGC 4191 both discs have similar populations; and the counter-rotating stars in IC 719 and NGC 448 are more metal rich than their main stellar discs. The duration of the accretion events can be also various that results in the different α-element to iron ratios. For instance, short time-scales result in the super-solar α-element to iron ratios in the counter-rotating stellar populations while prolonged formation of a counter-rotating component should produce a solar α/Fe abundance ratio and/or significant age gradient.

Nevertheless, for some targets the scenario of accretion from gas-rich neighbouring galaxies looks more plausible. For instance, no doubt that NGC 5719 and IC 719 have accreted their

counter-rotating stellar and gaseous discs from the closest neighbours because of the H I bridge (Vergani et al. 2007) between the galaxy and its neighbour, NGC 5713, in the case of NGC 5719, and the common H I envelope (Grossi et al. 2009) including both galaxies, in the case of IC 719 and its neighbour IC 718.

Recently, Coccato et al. (2015) have investigated the structure of the Virgo cluster S0 galaxy NGC 4191 by using the Integral field unit (IFU) spectroscopy obtained with the VIRUS-W spectrograph. They have interpreted the results of photometric as well as spectroscopic decomposition of NGC 4191 in the context of the recent cosmological simulation by Algorry et al. (2014), where it is demonstrated how distinct cosmological filamentary structures providing material with the opposite spins can finally produce two coplanar counter-rotating stellar discs. Coccato et al. (2015) found significant negative age gradients in both components of NGC 4191 correlating at least in the central 20 arcsec that indicates the inside-out formation of both components.

In our case of NGC 448, we observe a different situation. First, we show that the two independent approaches, the spectral and the photometric 2D decompositions, are in perfect agreement. The secondary counter-rotating disc reveals a detectable negative age gradient ($\Delta \log T_{CR} = -0.087 \pm 0.026$ dex dex^{-1}) that also gives an evidence for a prolonged inside-out formation process during approximately $3 \ldots 4$ Gyr. At the same time, the main stellar disc does not show any significant age gradient ($\Delta \log T_{MD} = -0.009 \pm 0.024$ dex dex^{-1}) that indicates that it was probably formed independently, by another mechanism than the secondary one. This is also supported by different metallicity gradients ($\Delta \log Z_{CR} = -0.09 \pm 0.04$ dex dex^{-1}, $\Delta \log Z_{MD} = -0.33 \pm 0.05$ dex dex^{-1}). Moreover, based on our stellar metallicity measurements, we suggest that the accreted gas was pre-enriched by metals in the companion galaxy and that the scenario of the counter-rotating disc formation from cosmological filaments is implausible for NGC 448.

Taking into account the large mass of the counter-rotating stellar population $M_{CR} = 9.0^{+2.7}_{-1.8} \times 10^9$ M$_\odot$ and indistinguishable properties of the stellar populations in the central region of the galaxy, we conclude that a significant fraction of accreted material had been already transformed into stars prior to the moment when the disc was acquired by NGC 448. All these observational facts indicate that the most probable formation scenario for the counter-rotating disc in NGC 448 is a merger event with a consequent prolonged gaseous accretion.

Remarkably, neither the search for emission lines of ionized gas in our optical spectra, nor attempts of radio observation of CO emission (Young et al. 2011) and H I 21-cm line yielded any detection of gas in NGC 448. Only IR image indirectly points to the probable presence of gas. The formation of its counter-rotating disc occurred approximately $6 \ldots 7$ Gyr ago since the remnants of the gas could be swept away by a recent tidal interaction between the galaxy and its satellite GALEXMSC J011516.31−013456.8 supported by the presence of a low surface brightness bridge connecting the two galaxies.

In conclusion, several recent studies, including ours, demonstrate that various scenarios to form counter-rotating stellar components can take place in real galaxies. It is important to expand the sample of disc galaxies with counter-rotation studied in detail, in order to produce quantitative conclusions on the probability of different formation scenarios supported by the statistics. The on-going large spectroscopic surveys of galaxies such as CALIFA (Sánchez et al. 2012), MANGA (Bundy et al. 2015), SAMI (Bryant et al. 2015) would help to compile a list of good candidates for subsequent

detailed studies. However, dedicated follow-up deep spectroscopic observations (IFU or long-slit) are required in order to obtain high-signal-to-noise ratios and also the appropriate spectral resolution in order for the spectral decomposition techniques to be successful.

REFERENCES

Afanasiev V. L., Moiseev A. V., 2005, Astron. Lett., 31, 194
Akaike H., 1974, IEEE Trans. Autom. Control, 19, 716
Alam S. et al., 2015, ApJS, 219, 12
Algorry D. G., Navarro J. F., Abadi M. G., Sales L. V., Steinmetz M., Piontek F., 2014, MNRAS, 437, 3596
Barnes J. E., Hernquist L. E., 1991, ApJ, 370, L65
Bertin E., 2011, in Evans I. N., Accomazzi A., Mink D. J., Rots A. H., eds, ASP Conf. Ser. Vol. 442, Astronomical Data Analysis Software and Systems XX. Astron. Soc. Pac., San Francisco, p. 435
Bertin E., Arnouts S., 1996, A&AS, 117, 393
Bryant J. J. et al., 2015, MNRAS, 447, 2857
Bundy K. et al., 2015, ApJ, 798, 7
Caldwell N., Rose J. A., Concannon K. D., 2003, AJ, 125, 2891
Cappellari M., Emsellem E., 2004, PASP, 116, 138
Cappellari M. et al., 2011, MNRAS, 413, 813
Chilingarian I., Prugniel P., Sil'Chenko O., Koleva M., 2007a, in Vazdekis A., Peletier R., eds, Proc. IAU Symp. 241, Stellar Populations as Building Blocks of Galaxies. Cambridge Univ. Press, Cambridge, p. 175
Chilingarian I. V., Prugniel P., Sil'Chenko O. K., Afanasiev V. L., 2007b, MNRAS, 376, 1033
Chilingarian I. V., Novikova A. P., Cayatte V., Combes F., Di Matteo P., Zasov A. V., 2009, A&A, 504, 389
Chilingarian I. V., Mieske S., Hilker M., Infante L., 2011, MNRAS, 412, 1627
Ciesla L. et al., 2014, A&A, 565, A128
Coccato L., Morelli L., Corsini E. M., Buson L., Pizzella A., Vergani D., Bertola F., 2011, MNRAS, 412, L113
Coccato L., Morelli L., Pizzella A., Corsini E. M., Buson L. M., Dalla Bontà E., 2013, A&A, 549, A3
Coccato L. et al., 2015, A&A, 581, A65

Corsini E. M., 2014, in Iodice E., Corsini E. M., eds, ASP Conf. Ser. Vol. 486, Multi-Spin Galaxies. Astron. Soc. Pac., San Francisco, p. 51

Crocker A. F., Jeong H., Komugi S., Combes F., Bureau M., Young L. M., Yi S., 2009, MNRAS, 393, 1255

de Vaucouleurs G., de Vaucouleurs A., Corwin H. G., Jr, Buta R. J., Paturel G., Fouqué P., 1991, Third Reference Catalogue of Bright Galaxies. Volume I: Explanations and references. Volume II: Data for galaxies between 0^h and 12^h. Volume III: Data for galaxies between 12^h and 24^h.

Duc P.-A. et al., 2015, MNRAS, 446, 120

Erwin P., 2015, ApJ, 799, 226

Evans N. W., Collett J. L., 1994, ApJ, 420, L67

Galletta G., 1996, in Buta R., Crocker D. A., Elmegreen B. G., eds, ASP Conf. Ser. Vol. 91, IAU Colloq. 157: Barred Galaxies. Astron. Soc. Pac., San Francisco, p. 429

Grossi M. et al., 2009, A&A, 498, 407

Häussler B. et al., 2007, ApJS, 172, 615

Johnston E. J., Merrifield M. R., Aragón-Salamanca A., Cappellari M., 2013, MNRAS, 428, 1296

Katkov I. Y., Chilingarian I. V., 2011, in Evans I. N., Accomazzi A., Mink D. J., Rots A. H., eds, ASP Conf. Ser. Vol. 442, Astronomical Data Analysis Software and Systems XX. Astron. Soc. Pac., San Francisco, p. 143

Katkov I., Chilingarian I., Sil'chenko O., Zasov A., Afanasiev V., 2011, Balt. Astron., 20, 453

Katkov I. Y., Sil'chenko O. K., Afanasiev V. L., 2013, ApJ, 769, 105

Katkov I. Y., Sil'chenko O. K., Afanasiev V. L., 2014, Astrophys. Bull., 69, 121

Krajnović D. et al., 2011, MNRAS, 414, 2923

Le Borgne D., Rocca-Volmerange B., Prugniel P., Lançon A., Fioc M., Soubiran C., 2004, A&A, 425, 881

McDermid R. M. et al., 2015, MNRAS, 448, 3484

Paturel G., Petit C., Prugniel P., Theureau G., Rousseau J., Brouty M., Dubois P., Cambrésy L., 2003, A&A, 412, 45

Peng C. Y., Ho L. C., Impey C. D., Rix H.-W., 2010, AJ, 139, 2097

Pizzella A., Corsini E. M., Vega Beltrán J. C., Bertola F., 2004, A&A, 424, 447

Pizzella A., Morelli L., Corsini E. M., Dalla Bontà E., Coccato L., Sanjana G., 2014, A&A, 570, A79

Prugniel P., Soubiran C., Koleva M., Le Borgne D., 2007, preprint (arXiv:astro-ph/0703658)

Puerari I., Pfenniger D., 2001, Ap&SS, 276, 909

Rines K., Geller M. J., Kurtz M. J., Diaferio A., 2003, AJ, 126, 2152

Rubin V. C., 1994, AJ, 108, 456

Sánchez S. F. et al., 2012, A&A, 538, A8

Schwarz G., 1978, Ann. Stat., 6, 461

Thakar A. R., Ryden B. S., 1996, ApJ, 461, 55

Thakar A. R., Ryden B. S., 1998, ApJ, 506, 93

Tohline J. E., Simonson G. F., Caldwell N., 1982, ApJ, 252, 92

van der Marel R. P., Franx M., 1993, ApJ, 407, 525

van Dokkum P. G., 2001, PASP, 113, 1420

Vergani D., Pizzella A., Corsini E. M., van Driel W., Buson L. M., Dettmar R.-J., Bertola F., 2007, A&A, 463, 883

Young L. M. et al., 2011, MNRAS, 414, 940

This paper has been typeset from a TEX/LATEX file prepared by the author.